COHERENT FINE-SCALE EDDY CLUSTER IN A TURBULENT MIXING LAYER

Yoshitsugu Naka

Department of Mechanical Engineering
Meiji University
1-1-1 Higashimita, Tama-ku, Kawasaki, Kanagawa, 214-8571, Japan
naka@meiji.ac.jp

Toshitaka Itoh*, Yuki Minamoto, Masayasu Shimura, Mamoru Tanahashi

Department of Mechanical Engineering
Tokyo Institute of Technology
2-12-1 Ookayama, Meguro-ku, Tokyo 152-8550, Japan
ito@g.ecc.u-tokyo.ac.jp

ABSTRACT

Clustering of coherent fine-scale structures in a turbulent mixing layer has been analyzed by a direct numerical simulation (DNS) data at $Re_\lambda \simeq 250$. The coherent fine-scale structures are extracted based on the second invariant of the velocity gradient tensor and the vorticity vector. Their characteristics are consistent with the lower Reynolds number data. The clustering is evaluated by the number density of coherent fine-scale eddies. The large-scale structures are extracted by low-pass filtering velocity data. The correlations between the number density and large-scale turbulence characteristics such as the enstrophy, the strain rate magnitude and the enstrophy amplification rate are investigated. The enstrophy is more correlated with the number density compared to the strain rate and the enstrophy amplification rate. Furthermore, the alignments of the vorticity vector and the eigenvectors of the large-scale strain rate tensor are evaluated. These alignment are computed by imposing a condition on the number density or the strain rate magnitude. The intense strain rate indicates the strong preferential alignment between the vorticity and the eigenvectors. On the other hand, the alignment becomes weaker in the high number density region of the fine-scale eddies. Finally, the inter-scale energy transfer is evaluated from the energy transfer between grid and subgrid scales. By definition, the significant positive correlation is observed in the magnitude of the strain rate and the inter-scale energy transfer while it is not much apparent with the number density.

INTRODUCTION

In the classical picture of turbulence, the kinetic energy is injected at a large-scale, and it is transferred through the inertial subrange down to small dissipative scales. This is hypothesized in physical space such that a large-scale eddy is broken into smaller ones until the energy is dissipated into heat. Such small-scale turbulence structures responsible for dissipation are represented by eddies with the most probable diameter of 8η (Tanahashi *et al.*, 1997, 2001; Wang *et al.*, 2007), and they are known as worms (Jiménez *et al.*, 1993). These small-scale turbulence structures exhibit universal characteristics in different flow types (Tanahashi *et al.*, 1997, 2001, 2004; Wang *et al.*, 2007). On the other hand, it is not straightforward to define turbulence structures responsible for the energy cascade in physical space. Leung *et al.* (2012) identified structures of different scales by using band pass filtering, and found that the energy cascade process is relevant to the vortex stretching by a slightly larger scale, which is consistent with the classical picture of energy cascade. They have also pointed out that small-scale structures tend to form clusters around a larger structure. The relation between the coherent fine-scale eddy cluster and the energy cascade in a homogeneous isotropic turbulence has been investigated by Tanahashi *et al.* (2008). Clustering of fine-scale eddies in the near wall region of the turbulent channel flow has also been revealed by Kang *et al.* (2007). Clustering of small-scale structures has been also found by Ishihara *et al.* (2013). The scale of the cluster is significantly larger than the Kolmogorov length scale and it has an order of the integral length scale.

The strain rate and the vorticity are two fundamental quantities to describe the dynamics of turbulence. Buxton *et al.* (2011) analyzed their interaction based on the transport equations of the enstrophy and the magnitude of the strain rate tensor. The key quantity is that the production term in the enstrophy equation, $\omega_i S_{ij} \omega_j$, where $\omega_i = \varepsilon_{ijk} W_{jk}$ is the vorticity vector, S_{ij} is the strain rate tensor and W_{ij} is the rotation rate tensor. Fiscaletti *et al.* (2016) investigated scale interactions by amplitude modulation analyses.

The present study analyzes the large-scale clustering of coherent fine-scale structures using a numerical database of a temporally developing turbulent mixing layer. A DNS at the turbulent Reynolds number $Re_\lambda \simeq 250$ has been performed. The degree of clustering fine-scale turbulence is measured by the number density of the coherent fine-scale eddies. The large-scale strain and vorticity fields are obtained by applying low-pass filtering. The relation between the large-scale structures of the strain and the vorticity field, and clustering of the fine-scale turbulence structures is quantified.

DNS OF A TURBULENT MIXING LAYER

A DNS of a temporally developing turbulent mixing layer has been performed. The solver was originally developed and reported in our previous study (Tanahashi *et al.*, 2001). Variables in the streamwise and spanwise directions are expanded into Fourier series and into sine/cosine series in the transverse direction. The time integration is conducted by the low-storage third-order Runge-Kutta scheme. The boundary conditions are periodic in the streamwise and spanwise directions, and free-slip in the transverse direction. The initial mean velocity distribution is given by a hyperbolic tangent profile: $\tilde{u}(y) = 0.5 \tanh(2y)$, and the small random perturbations are superposed. The dimensions of computational domain are set to be $4\Lambda \times 6\Lambda \times 8/3\Lambda$, where Λ is the most unstable wave-

*Present affiliation: Department of Aeronautics and Astronautics, The University of Tokyo, 7-3-1 Hongo, Bunkyo-ku, Tokyo 113-8656, Japan

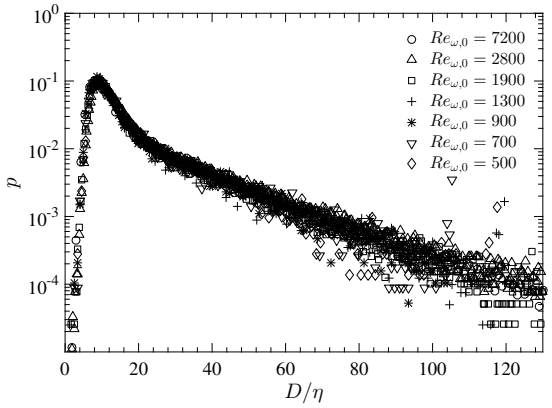

Figure 1. PDF of the diameter of the coherent fine-scale eddy.

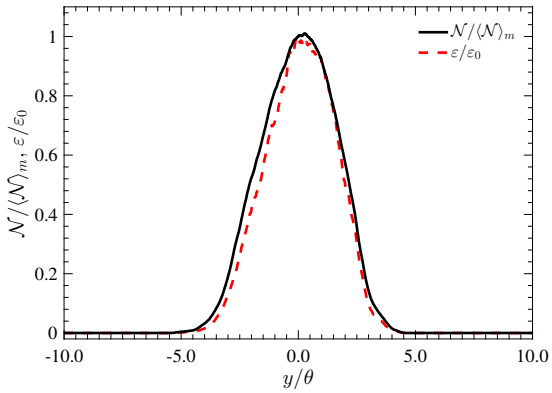

Figure 2. Profile of the number density of the coherent fine-scale eddy and the normalized energy dissipation rate.

length. The Reynolds number based on the initial vorticity thickness ($Re_{\omega,0}$) is 7200. The number of grid points is $1728\times2593\times1152$. The simulation has been carried out until the sub-harmonic mode had been fully developed (t = 150). The velocity field at t = 135 is used for the present analyses. The turbulent Reynolds number Re_λ reaches approximately 250 in the fully developed state. It is noted that Re_λ achieved is among the highest in this type of flow to date. The computation has been conducted using the NEC SX-ACE system at Tohoku University, consuming 144 cores and about 21 $\times10^3$ CPU hours.

The fundamental statistics such as the mean velocity and the velocity fluctuations of the present simulation exhibit a good agreement with those of the previous study in the literature (for example, Rogers & Moser (1994)). The resolution is confirmed that $k_{\max}\eta \sim 1.5$, where $k_{\max}$ is the maximum wavelength and η is the Kolmogorov length scale. These results confirm that the present DNS gives a reliable database of a turbulent mixing layer.

Coherent fine-scale eddies are extracted using the method similar to our previous studies (Tanahashi *et al.*, 1997, 2001). It is based on the second invariant of the velocity gradient tensor $Q = (1/2)(W_{ij}W_{ij} - S_{ij}S_{ij})$, and the axis of the eddy is defined by the vorticity vector. 1.36 million fine-scale eddies are extracted in a snapshot at t = 135. Figure 1 shows the probability density function (PDF) of the diameter of the coherent fine-scale eddy. It is confirmed that the present result is consistent with the data at lower Reynolds numbers in our previous studies (Tanahashi *et al.*, 1997, 2001; Wang *et al.*, 2007).

To extract large-scale turbulence structures, the velocity field is low-pass filtered using a Gaussian kernel with a filter width of Δ. In the present paper, results with the filter width at $\Delta = 160\eta$ is shown. This filter width can be compared with the integral length scale $l = 502\eta$ and the Taylor micro scale $\lambda = 33.1\eta$.

FINE-SCALE EDDY CLUSTER AND TURBULENCE QUANTITIES

Clustering is measured by the number density of coherent fine-scale eddies $\mathcal{N} = n/V$, where n is the number of coherent fine-scale eddies within a control volume V of which size is $(40\eta)^3$. Figure 2 shows profiles of $\mathcal{N}/\langle\mathcal{N}\rangle_m$ and the energy dissipation rate $\varepsilon/\varepsilon_0$ across the mixing layer. These values are normalized by the averaged value at the center of the mixing layer. The profile shows a peak at the center, and the high number density region having high energy dissipation rate is well defined.

To link fine-scale eddy clusters and turbulence quantities, the joint PDF of the number density $\mathcal{N}$ and the enstrophy $\langle\omega^2\rangle_V$, and that of $\mathcal{N}$ and the strain rate $\langle S_{ij}S_{ij}\rangle_V$ are computed. $\langle\rangle_V$ indicates that the quantities are spatially averaged within the same control

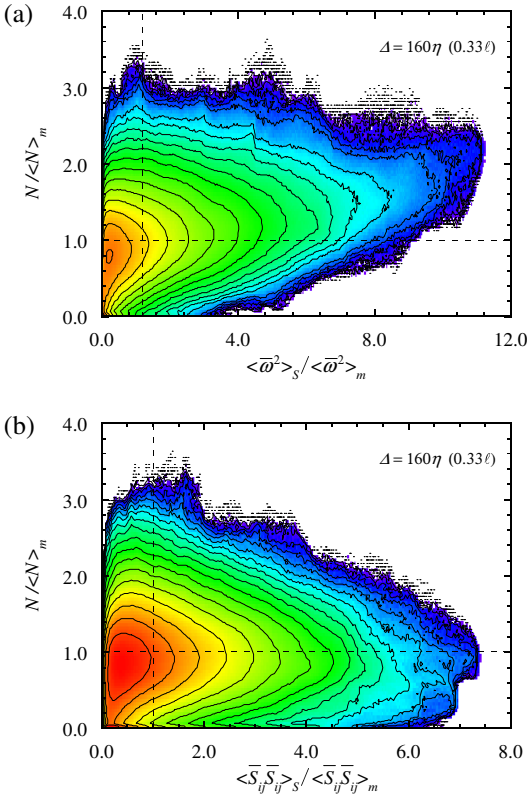

Figure 3. Joint p.d.f. between $\mathcal{N}/\langle\mathcal{N}\rangle_m$ and enstrophy (a) and $\mathcal{N}/\langle\mathcal{N}\rangle_m$ and the strain rate magnitude (b) of filtered data at $\Delta = 160\eta$.

volume as the number density. The joint PDF of $\mathcal{N}$ and $\langle\overline{\omega^2}\rangle_V$, and that of $\mathcal{N}$ and $\langle\overline{S_{ij}S_{ij}}\rangle_V$ are shown in Fig. 3. The distributions of these PDFs are apparently different especially for high number density condition ($\mathcal{N} > 2.0$). The PDF of the enstrophy indicates that the probability of the stronger enstrophy is maintained for the high population condition. On the other hand, the PDF of the strain rate indicates that the correlation of the high magnitude of large-scale strain and the high number density of the eddies is not apparent. This gives an idea of the spatial distributions of the fine-scale eddy cluster and large-scale turbulence structures. The intense enstrophy structures tend to exist in the high density region of the fine-scale eddies, while the strain rate structures are not active as much within

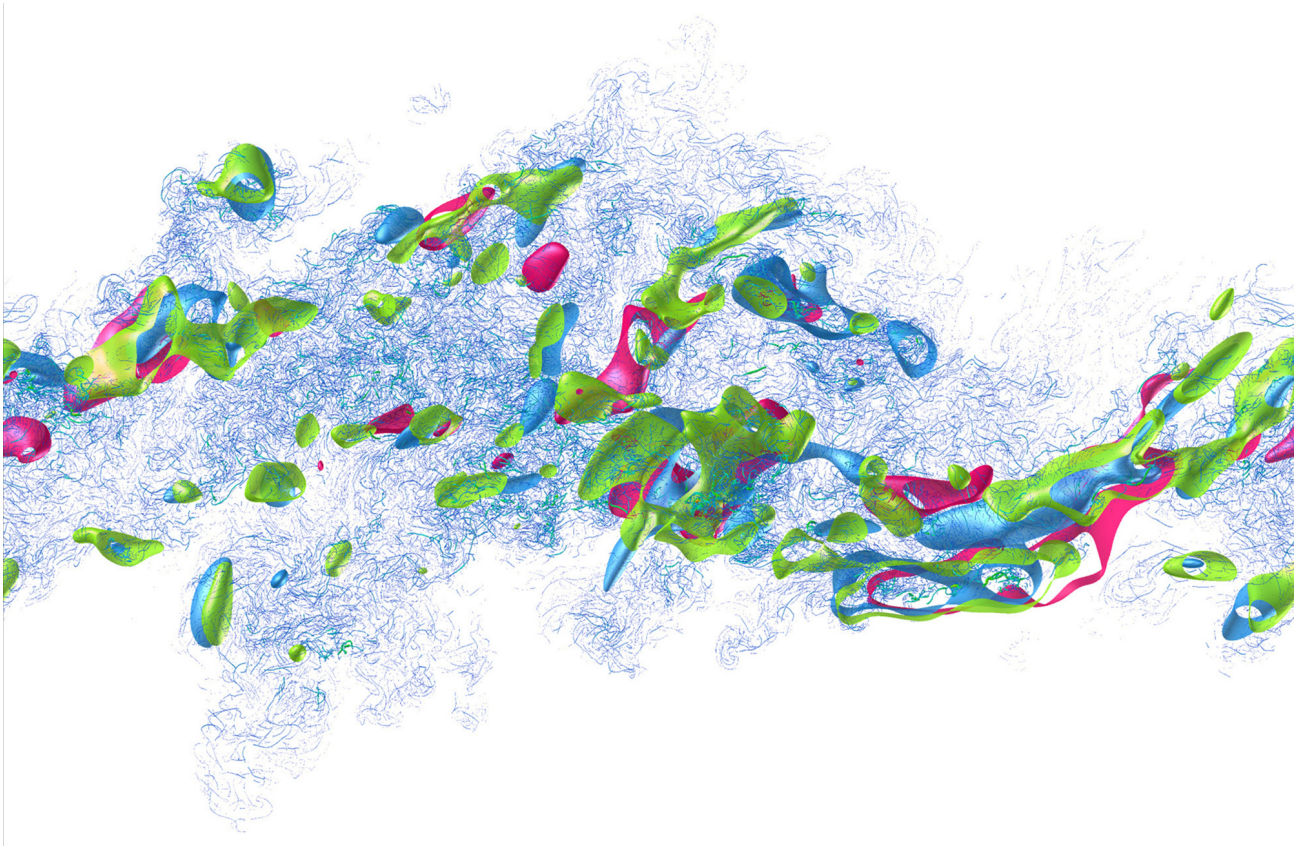

Figure 4. Snapshot of large-scale $\overline{\omega^2}$ (blue), $\overline{S_{ij}S_{ij}}$ (magenta) and $\overline{\omega_i}\overline{S_{ij}}\overline{\omega_j}$ (green) structures overlaid on the clusters of coherent fine-scale eddies.

the cluster. It is noted that the p.d.f.s of the unfiltered enstrophy and strain rate are very similar and both show very strong correlations with $\mathcal{N}$ (not shown) since they include small scale contributions created by fine-scale eddies themselves. In addition, as it is indicated in figure 2, high number density corresponds to high energy dissipation.

In the transport equations of the enstrophy and the strain rate magnitude, the enstrophy amplification term $\omega_i S_{ij} \omega_j$ represents the gain and loss of the enstrophy and the strain rate magnitude, respectively. Therefore, looking at the relation of these three terms is of our interest. Figure 4 shows instantaneous isosurfaces of these terms superposed on the axes of coherent fine-scale eddies. The enstrophy, the strain rate and the amplification of enstrophy are filtered at $\Delta = 160\eta$. The threshold values are chosen to be 1.8 times of the mean value at the center of the shear layer ($y = 0$) so that large-scale intense structures can be identified. Thickness and color of the axes are scaled by their magnitude of Q. Strong eddies are illustrated as thick red axes, whilst weak ones are depicted as thin blue axes. The visualized field is a thin slab with spanwise length of $L_z/24$ ($= 4.6\lambda$). The large-scale intense enstrophy structures exist near the populated region of eddies. The strain rate tends to locate in relatively sparse region. It is also found that fine-scale eddy axes distribute off-center of large-scale strong enstrophy structures, which is consistent with Leung *et al.* (2012). In terms of spatial relation between the large-scale enstrophy and strain rate structures, they tend to exist close to each other. In addition, the intense enstrophy amplification structures locate between these two, which play a role in an exchange between the enstrophy and the strain rate. These observations qualitatively suggest interactions between these terms in the physical space.

Figure 5 presents the filtered enstrophy $\langle\overline{\omega^2}\rangle_V$, strain rate magnitude $\langle\overline{S_{ij}S_{ij}}\rangle_V$ and amplification rate of the enstrophy $\langle\overline{\omega_i}\overline{S_{ij}}\overline{\omega_j}\rangle_V$ conditionally averaged on the number density of the coherent fine-scale eddies $\mathcal{N}$. The enstrophy constantly increases with $\mathcal{N}$, but the strain rate stays a value around average through from intermediate to high $\mathcal{N}$ regions. The enstrophy amplification term shows a noticeable tendency. It increases up to $\mathcal{N}/\langle\mathcal{N}\rangle_m \simeq 1.8$, and then drops until $\mathcal{N}/\langle\mathcal{N}\rangle_m \simeq 2.5$. This result implies that in the region where the coherent fine-scale eddies are moderately populated, i.e., $1.0 \leq \mathcal{N}/\langle\mathcal{N}\rangle_m \leq 1.8$, the large-scale enstrophy amplification is active whereas in the region where the coherent fine-scale eddies are highly populated, that is, in the clusters, the enstrophy amplification at large-scale becomes weaker. If it is supposed to take vortex stretching as a principal mechanism for en-

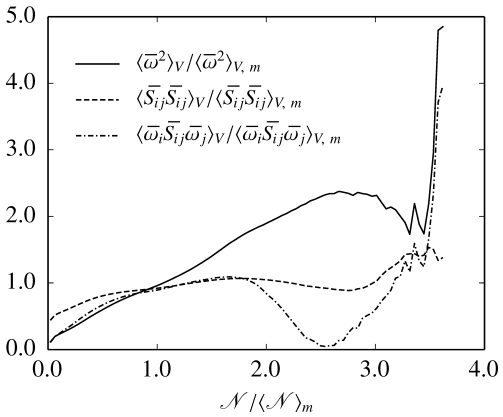

Figure 5. Averaged $\langle\overline{\omega^2}\rangle_V$, $\langle\overline{S_{ij}S_{ij}}\rangle_V$ and $\langle\overline{\omega_i}\overline{S_{ij}}\overline{\omega_j}\rangle_V$ conditioned by $\mathcal{N}$.

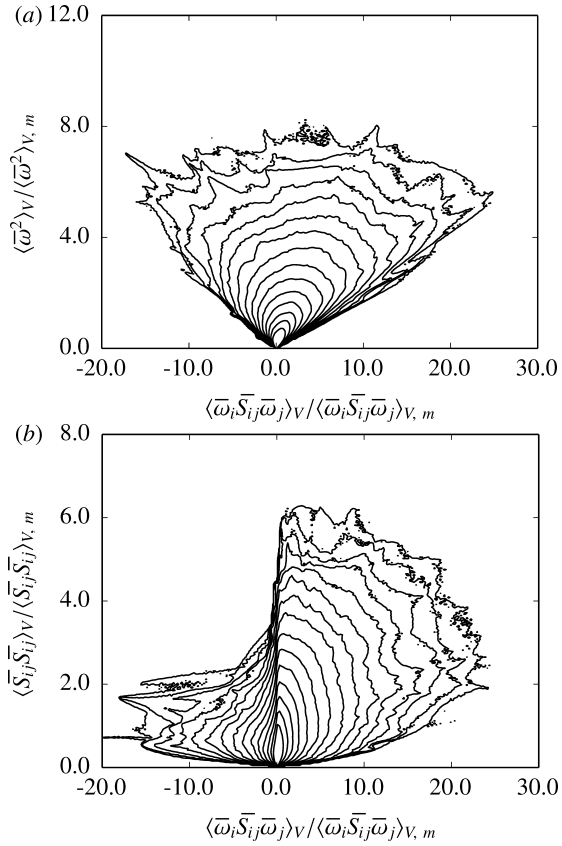

Figure 6. joint p.d.f.s between (a) $\langle\overline{\omega_i}\overline{S_{ij}}\overline{\omega_j}\rangle_V$ and $\langle\overline{\omega^2}\rangle_V$, and (b) $\langle\overline{\omega_i}\overline{S_{ij}}\overline{\omega_j}\rangle_V$ and $\langle\overline{S_{ij}S_{ij}}\rangle_V$. The inner contour level is -2 and the outer contour level is -16.

strophy amplification as discussed by (Hamlington *et al.*, 2008), the result in figure 5 indicates that the large-scale vortex stretching is significantly reduced in the clusters. For higher number density $2.5 \leq \mathcal{N}/\langle\mathcal{N}\rangle_m \leq 3.0$, however, the data behave differently: the enstrophy stops increasing and the enstrophy amplification re-increases. For the current database, the number of samples for $\mathcal{N}/\langle\mathcal{N}\rangle_m > 3.0$ may not be sufficient to discuss the meaning of this behavior. Therefore it is desired to have higher Reynolds number data showing higher intermittency. It is also noted that these quantities increase monotonically with $\mathcal{N}$ for the unfiltered data. This can be interpreted as a result of strain rate field induced by small-scale vortices within high $\mathcal{N}$ region.

After looking at the effect of population density, the relationship of the enstrophy and strain rate fields against the enstrophy amplification is considered. Figure 6 indicates the joint p.d.f.s of (a) $\langle\overline{\omega_i}\overline{S_{ij}}\overline{\omega_j}\rangle_V$ and $\langle\overline{\omega^2}\rangle_V$ and (b) $\langle\overline{\omega_i}\overline{S_{ij}}\overline{\omega_j}\rangle_V$ and $\langle\overline{S_{ij}S_{ij}}\rangle_V$. For large-scale structures, the negative enstrophy amplification is not associated with the strong strain rate event whereas the intense enstrophy event is significantly correlated with both negative and positive enstrophy amplification. This indicates that large-scale intense strain plays an important role in positive enstrophy amplification. Buxton & Ganapathisubramani (2010) showed that the enstrophy production ($\omega_i S_{ij}\omega_j > 0$) is caused by parallel alignment of the vorticity vector with the extensional eigenvector of the strain rate tensor. From this view point, the finding in figure 6(b) would be a signature of the parallel alignment of the vorticity vector with the extensional strain rate eigenvector caused by large-scale intense strain field.

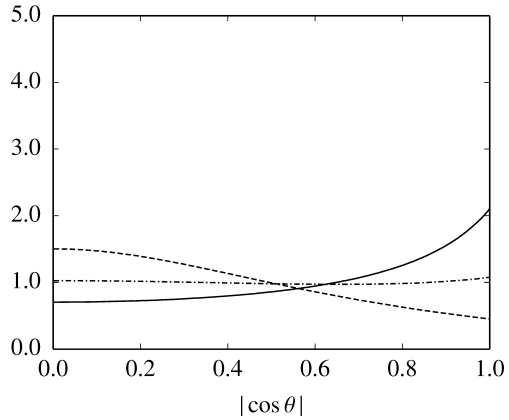

Figure 7. Alignment of the vorticity vector and the eigenvectors of the strain rate tensor for (a) the unfiltered strain field and (b) the filtered strain field for $\Delta = 160\eta$.

ALIGNMENT OF THE VORTICITY VECTOR AND THE EIGENVECTORS OF THE STRAIN RATE TENSOR

The enstrophy amplification term is a key quantity contributing both the enstrophy and the strain rate. The magnitude of this term strongly depends on the alignment of the strain rate tensor and the vorticity vector as described by the following relation: $\omega_i S_{ij}\omega_j = \omega^2 s_i(\hat{e_i}\cdot\hat{\omega})^2$, where $\omega^2 = \omega_i\omega_i$, s_i is the eigenvalue of S_{ij}, $\hat{e_i}$ is its eigenvector and $\hat{\omega} = \omega/|\omega|$. The alignment of the strain rate and the vorticity has been extensively investigated. The preferential alignment of the vorticity vector with the intermediate eigenvector has previously been observed numerically (Ashurst *et al.*, 1987; Vincent & Meneguzzi, 1994; Tanahashi *et al.*, 2001) and experimentally (Tsinober *et al.*, 1992; Mullin & Dahm, 2006; Naka *et al.*, 2016). On the other hand, based on the classical picture of turbulence, the vortices exerted to the shear are likely to be aligned in its direction. Hamlington *et al.* (2008) examined the local and non-local effects of strain rate field by dividing physical space with a cutoff radius and showed that vorticity vector preferentially aligns with the extensional strain rate in the non-local field. Leung *et al.* (2012) confirmed this by filtering out the local strain field by bandpass filtering. They adopted a somewhat larger filter width for the strain rate field than that for the enstrophy field, by which the non-local effect of strain rate can be extracted.

Figure 7 presents the p.d.f. of alignment cosine of the vorticity vector and the eigenvectors of the strain rate tensor. The strain rate is filtered at $\Delta = 160\eta$. The vorticity vector preferentially aligns with the most extensional eigenvector rather than the intermediate one. This is due to filtering out the local strain rate field as noted by Leung *et al.* (2012). Therefore, it is considered that this filter width is adequate to see the alignment of the vorticity vector and the most extensional eigenvector of the filtered strain rate.

Figure 8 shows the alignment of the vorticity with the strain rate eigenvector conditioned by the number density of coherent fine-scale eddy $\mathcal{N}$. In the moderate density region such that $\mathcal{N}/\langle\mathcal{N}\rangle_m < 2.0$ (figure 8a), the p.d.f.s of the alignment cosine are quantitatively similar to those in figure 7. On the other hand, in the highly populated region, $2.0 \leq \mathcal{N}/\langle\mathcal{N}\rangle_m < 3.0$ (figure 8b), the p.d.f.s become flat suggesting that the alignment of the vortices and large-scale strain rate inside the clusters are less directional. This finding highlights the result in figure 5 which shows that the large-scale enstrophy amplification is relatively small in the cluster.

Figure 9 shows the alignment of vorticity and the eigenvectors of the strain rate conditioned by the strain rate magnitude. To see the contribution of the intense strain rate, the alignment p.d.f. is conditioned by the strain rate magnitude. The shape of the p.d.f. is

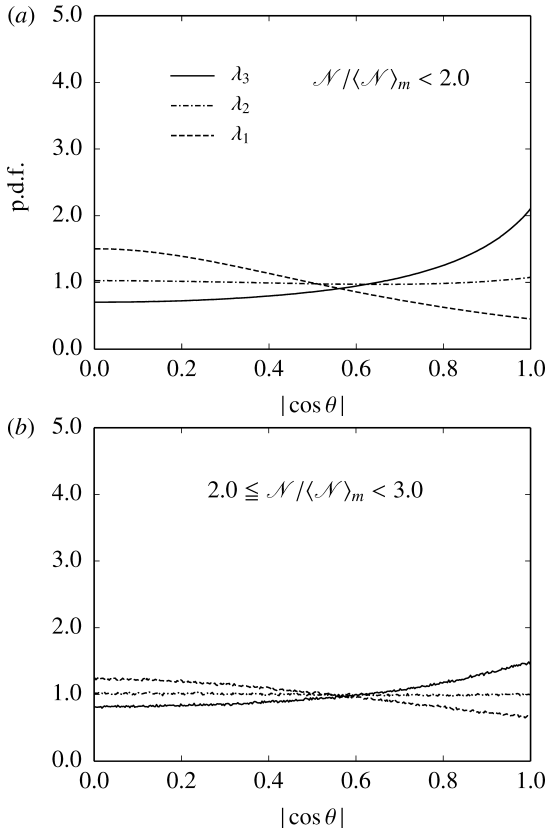

Figure 8. Alignment of the eigenvectors of the strain rate tensor and the vorticity vector for different number density conditions; (a) $\mathcal{N}/\langle\mathcal{N}\rangle_m < 2.0$, (b) $2.0 \leq \mathcal{N}/\langle\mathcal{N}\rangle_m < 3.0$.

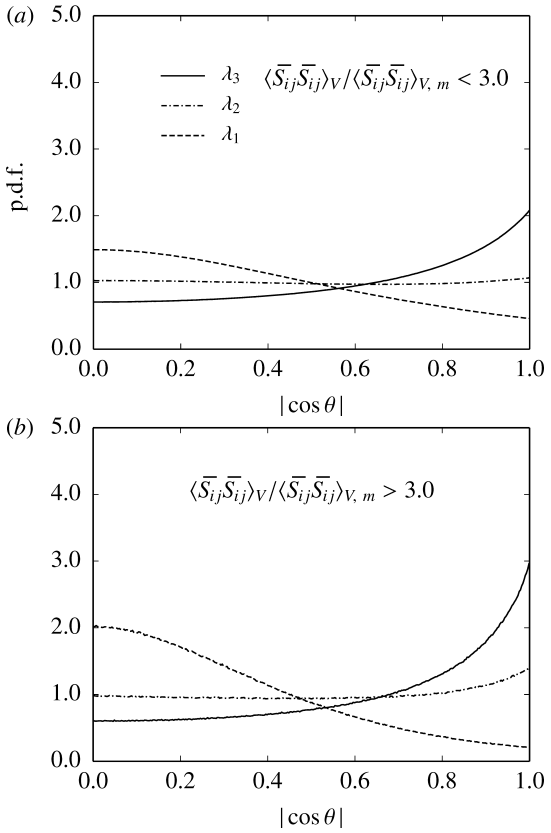

Figure 9. Alignment of the eigenvectors of the strain rate tensor and the vorticity vector for different strain rate conditions; (a) $\langle S_{ij}S_{ij}\rangle_V/\langle S_{ij}S_{ij}\rangle_{V,m} < 3.0$, (b) $\langle S_{ij}S_{ij}\rangle_V/\langle S_{ij}S_{ij}\rangle_{V,m} \geq 3.0$.

in general the same with figure7 for the both cases. However, the peaks of p.d.f.s for λ_3 and λ_1 in figure 9(b) are much more pronounced around $|\cos\theta| = 1$ and $|\cos\theta| = 0$ respectively, than that in figure 9(a). This suggests that within intense strain rate region, the vorticity is predominantly perpendicular to the compressive strain rate and parallel to the extensional one. This is closely related to the results shown in figure 6(b). The strong strain rate selectively gives the enstrophy production. These evidences lead to an assumption that the clusters of fine-scale structures can be formed and maintained by associating intense strain rate structures located in the periphery of the cluster, in which prevalent formation of worm-like vortices occurs as a result of the preferential alignment of vorticity with the largest extensional strain rate.

INTER-SCALE ENERGY TRANSFER

The inter-scale energy transfer is fundamental phenomenon in turbulence. In the framework of LES, it is important to know the energy transfer between the grid scale (GS) and subgrid scale (SGS) motions. The energy transfer is quantitatively represented by the GS-SGS energy transfer term, $E_\tau = -\tau_{ij}S_{ij}$, where τ_{ij} is the SGS stress tensor.

Importance of intense strain rate on the inter-scale energy transfer is confirmed by figure 10(a) which shows the joint p.d.f. of $\langle E_\tau\rangle_V$ and $\langle S_{ij}S_{ij}\rangle_V$ at filter size of $\Delta = 160\eta$. The energy transfer and the strain rate show a strong positive correlation. Intense strain rate leads to high value of forward energy transfer whereas moderate strain is accompanied with both forward and backward energy transfer. The definition of E_τ partially explains this result: larger magnitude of S_{ij} leads to larger magnitude of E_τ, although it gives no explanation for the positive correlation between E_τ and $S_{ij}S_{ij}$. This result can be understood by recalling the alignment of the vorticity with the principal strain rate suggested in figure 9. In the intense strain rate region the vorticity preferentially aligns with the most extensional strain rate leading to the dominance of vortex stretching and the forward energy transfer. On the other hand, within the moderate strain rate region the preferential alignment becomes weaker, resulting in moderate forward energy transfer and appearance of backward energy transfer.

Figure 10(b) represents the joint p.d.f. of $\langle E_\tau\rangle_V$ and the number density of fine-scale eddies $\mathcal{N}$. The forward energy transfer can take significant value for $\mathcal{N}/\langle\mathcal{N}\rangle_m \sim 1.0$, while in the high density region, the most probable amount of energy transfer is around average. This suggests that active energy transfer does not take place within the fine-scale eddy clusters, as expected from the result of figure 8(b). In that region, the principal action is energy dissipation. Since creation of small-scale vortices by large-scale strain rate would take some time, it is not surprising that the region of active energy transfer does not correspond to an high eddy number density region at an instantaneous flow field.

CONCLUSION

A direct numerical simulation of a temporally developing turbulent mixing layer at $Re_\lambda \simeq 250$ has been conducted. Coherent fine-scale eddies are extracted from the DNS data, and their number density is defined to measure clustering of the fine-scale eddies. The large-scale structures are separated using a Gaussian low-pass filter. The relation between the fine-scale eddy cluster and the large-scale vorticity, and that with the strain rate are evaluated by the joint p.d.f. It indicates that the large-scale high enstrophy regions clearly correlate with the cluster of fine-scale eddies compared to the large-scale high strain-rate.

Interaction between enstrophy and strain rate fields is investi-

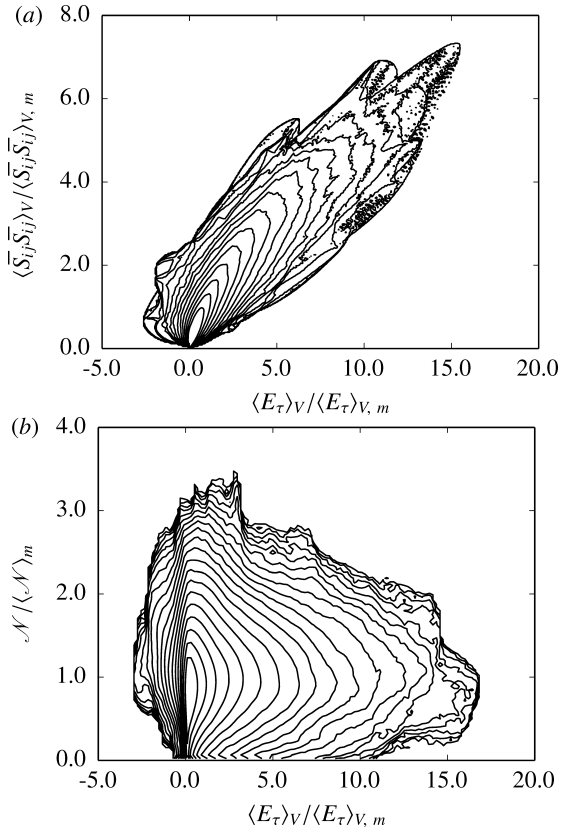

Figure 10. (a) Joint p.d.f. between $\langle E_\tau\rangle_V$ and $\langle\overline{S_{ij}S_{ij}}\rangle_V$. The inner contour level is -17 and the outer contour level is 1. (b) joint p.d.f. $\langle E_\tau\rangle_V$ and $\mathcal{N}$. The inner contour level is -20 and the outer contour level is 1.

gated in terms of the enstrophy amplification rate. In the instantaneous snapshot of isosurfaces, the large-scale enstrophy and strain rate structures exist close to each other, and that of the enstrophy amplification tends to exist in between. The large-scale enstrophy amplification within the high number density region is significantly reduced. It implies that vortex stretching by large-scale structure becomes weaker in the clusters. It is also found that the intense strain rate leads to the positive enstrophy amplification.

The p.d.f.s of the alignment cosine of the vorticity vector and the eigenvectors of the large-scale strain rate tensor are evaluated. The p.d.f. indicates flat shape in the high number density region, suggesting that the vortex stretching and compression are less directional. The p.d.f. conditioned by the magnitude of strain rate tensor is also evaluated and it is confirmed that the preferential alignment of vorticity with the most extensional strain becomes more prominent in the intense strain rate region.

The inter-scale energy transfer between grid and subgrid scales is investigated. High number density region does not correspond to the high energy transfer region, while the strain rate exhibits strong positive correlation with it. These results suggest that the strong strain rate structures play a role of active forward energy transfer. The vorticity vector preferentially aligns with the most extensional strain rate eigenvectors.

REFERENCES

Ashurst, W.T., Kerstein, A.R., Kerr, R.M. & Gibson, C.H. 1987 Alignment of vorticity and scalar gradient with strain rate in simulated Navier–Stokes turbulence. *Physics of Fluids* **30** (8), 2343–2353.

Buxton, O.R.H. & Ganapathisubramani, B. 2010 Amplification of enstrophy in the far field of an axisymmetric turbulent jet. *Journal of Fluid Mechanics* **651**, 483.

Buxton, O.R.H., Laizet, S. & Ganapathisubramani, B. 2011 The interaction between strain-rate and rotation in shear flow turbulence from inertial range to dissipative length scales. *Physics of Fluids* **23** (6), 061704.

Fiscaletti, D., Attili, A., Bisetti, F. & Elsinga, G. E. 2016 Scale interactions in a mixing layer - the role of the large-scale gradients. *Journal of Fluid Mechanics* **791**, 154–173.

Hamlington, P.E., Schumacher, J. & Dahm, W.J.A. 2008 Direct assessment of vorticity alignment with local and nonlocal strain rates in turbulent flows. *Physics of Fluids* **20**, 111703.

Ishihara, T., Kaneda, Y. & Hunt, J.C.R. 2013 Thin shear layers in high reynolds number turbulence? DNS results. *Flow, Turbulence and Combustion* **91** (4), 895–929.

Jiménez, J., Wray, A. A., Saffman, P. G. & Rogallo, R. S. 1993 The structure of intense vorticity in isotropic turbulence. *Journal of Fluid Mechanics* **255**, 65–90.

Kang, S.-J., Tanahashi, M. & Miyauchi, T. 2007 Dynamics of fine scale eddy clusters in turbulent channel flows. *Journal of Turbulence* **8**, N52.

Leung, T., Swaminathan, N. & Davidson, P.A. 2012 Geometry and interaction of structures in homogeneous isotropic turbulence. *Journal of Fluid Mechanics* **710**, 453–481.

Mullin, J.A. & Dahm, W.J.A. 2006 Dual-plane stereo particle image velocimetry measurements of velocity gradient tensor fields in turbulent shear flow. I. accuracy assessments. *Physics of Fluids* **18**, 035101.

Naka, Y., Tomita, K., Shimura, M., Fukushima, N., Tanahashi, M. & Miyauchi, T. 2016 Quad-plane stereoscopic PIV for fine-scale structure measurements in turbulence. *Experiments in Fluids* **57** (5), 1–20.

Rogers, M.M. & Moser, R.D. 1994 Direct simulation of a self-similar turbulent mixing layer. *Physics of Fluids* **6** (2), 903–923.

Tanahashi, M., Fujibayashi, K. & Miyauchi, T. 2008 Fine scale eddy cluster and energy cascade in homogeneous isotropic turbulence. In *IUTAM Symp. Computational Physics and New Perspectives in Turbulence*, pp. 67–72. Springer.

Tanahashi, M., Iwase, S. & Miyauchi, T. 2001 Appearance and alignment with strain rate of coherent fine scale eddies in turbulent mixing layer. *Journal of Turbulence* **2** (6), 1–18.

Tanahashi, M., Kang, S.-J., Miyamoto, T., Shiokawa, S. & Miyauchi, T. 2004 Scaling law of fine scale eddies in turbulent channel flows up to Re_τ = 800. *International Journal of Heat and Fluid Flow* **25**, 331–340.

Tanahashi, M., Miyauchi, T. & Ikeda, J. 1997 Identification of coherent fine scale structure in turbulence. In *IUTAM Symposium on Simulation and Identification of Organized Structures in Flows*, vol. 52, pp. 131–140.

Tsinober, A., Kit, E. & Dracos, T. 1992 Experimental investigation of the field of velocity gradients in turbulent flows. *Journal of Fluid Mechanics* **242**, 169–192.

Vincent, A. & Meneguzzi, M. 1994 The dynamics of vorticity tubes in homogeneous turbulence. *Journal of Fluid Mechchanics* **258**, 245–254.

Wang, Y., Tanahashi, M. & Miyauchi, T. 2007 Coherent fine scale eddies in turbulence transition of spatially-developing mixing layer. *International Journal of Heat and Fluid Flow* **28**, 1280–1290.